

studies<sup>13</sup>. However, other indirect growth studies performed in typical deep-sea habitats indicate that many invertebrate megabenthos grow at rates similar to those in the vents and not much lower than those in shallow water<sup>14–18</sup>.

Several small deep-sea species have high rates of growth and early maturation when presented with an appropriate food source<sup>2</sup> or vacant habitat<sup>19,20</sup> and some respond rapidly to natural deposition of food<sup>21,22</sup>. However, influences on the megafauna have previously been inferred only from the annual periodicity in the reproductive cycles of a few species<sup>19</sup>. The present data provide direct evidence that at least one megafaunal species grows rapidly in its natural habitat and can respond quickly to elevated food input by increasing its growth rate several times. □

Received 29 January; accepted 12 April 1990.

1. Turekian, K. K. *et al.* **72**, 2829–2832 (1975).
2. Turner, R. D. *Science* **180**, 1377–1379 (1973).
3. Hutchings, J. A. & Haedrich R. L. *Mar. Ecol. Prog. Ser.* **17**, 135–142 (1984).
4. Rhoads, D. C., Lutz, R. A., Revelas, E. C. & Cerrato, R. M. *Science* **214**, 911–912 (1981).
5. Lampitt, R. S. & Burnham M. P. *Deep Sea Res.* **30**, 1009–1017 (1983).
6. Bertalanffy, L. von *Am. Nat.* **85**, 111–117 (1951).
7. *SAS Users Guide (Version V)* (SAS Institute Inc., Cary, North Carolina, USA, 1985).
8. Williams, R. & Moyle, J. *J. crust. Biol.* **8**(2), 177–186 (1988).
9. Eckert, K. L. & Eckert S. A. *J. crust. Biol.* **7**(4), 682–690 (1987).
10. Billett, D. S. M., Lampitt, R. S., Rice, A. L. & Mantoura, R. F. C. *Nature* **302**, 520–522 (1983).
11. Lampitt, R. S. *Deep Sea Res.* **32**, 885–897 (1985).
12. Lutz, R. A., Fritz, L. W. & Rhoads, D. C. *Biol. Soc. Wash. Bull.* **6**, 199–210 (1985).
13. Grassie, J. F. *Nature* **265**, 618–619 (1977).
14. Gage, J. D., Tyler, P. A. & Nichols, D. *J. exp. mar. Biol. Ecol.* **101**, 61–83 (1986).
15. Nichols, D., Sime, A. A. T. & Bishop, G. M. *J. exp. mar. Biol. Ecol.* **66**, 219–228 (1985).
16. Gage, J. D. & Tyler, P. A. *Mar. Biol.* **90**, 41–43 (1985).
17. Gage, J. D. *Mar. Biol.* **96**, 19–30 (1987).
18. Gage, J. D. & Tyler, P. A. *Oceanologica Acta* **5**, 73–83 (1982).
19. Scheltema, A. H. *Mar. Ecol. Prog. Ser.* **37**, 171–180 (1987).
20. Desbruyeres, D., Bervas, J. Y. & Khrifounoff, A. *Oceanologica Acta* **3**, 285–291 (1980).
21. Gooday, A. J. *Nature* **232**, 70–73 (1988).
22. Lochte, K. & Turley, C. M. *Nature* **333**, 67–69 (1988).

ACKNOWLEDGEMENTS. I thank Drs M. V. Angel, D. S. M. Billett, M. J. R. Fasham and A. L. Rice for their comments on the manuscript, I. Waddington, G. R. J. Phillips, N. J. Griffin and I. Chapman for technical assistance, and the masters and crews of RRS *Challenger* and RRS *Discovery*.

## Postsynaptic NMDA receptor-mediated calcium accumulation in hippocampal CA1 pyramidal cell dendrites

Wade G. Regehr & David W. Tank\*

Biophysics Research Department, AT&T Bell Laboratories, Murray Hill, New Jersey 07974, USA

**IN the CA1 hippocampal region, intracellular calcium is a putative second messenger<sup>1,2</sup> for the induction of long-term potentiation (LTP), a persistent increase of synaptic transmission produced by high frequency afferent fibre stimulation<sup>3</sup>. Because LTP in this region is blocked by the NMDA (*N*-methyl-D-aspartate) receptor antagonist AP5 (DL-2-amino-5-phosphonovaleric acid) (ref. 4) and the calcium permeability of NMDA receptors is controlled by a voltage-dependent magnesium block<sup>5,6</sup>, a model has emerged that suggests that the calcium permeability of NMDA receptor-coupled ion channels<sup>7–10</sup> is the biophysical basis for LTP induction<sup>11–15</sup>. We have performed microfluorometric measurements<sup>16</sup> in individual CA1 pyramidal cells during stimulus trains that induce LTP. In addition to a widespread component of postsynaptic calcium accumulation previously described<sup>17</sup>, we now report that brief high frequency stimulus trains produce a transient component spatially localized to dendritic areas near activated afferents. This localized component is blocked by the NMDA receptor antagonist**

\* To whom correspondence should be addressed.

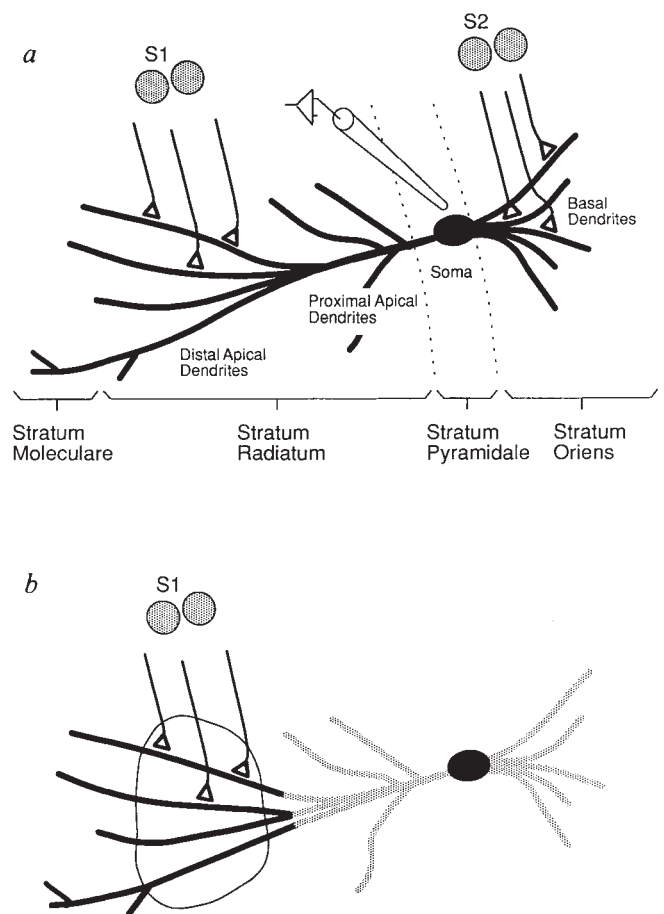


FIG. 1 Cell-electrode geometry. *a*, Stimulus electrodes positioned in stratum radiatum (electrode S1; distal apical dendrites) or stratum oriens (electrode S2; basal dendrites) activated a group of afferent fibres with average orientation parallel to the cell body layer. An extracellular electrode near the cell soma recorded the population spike. *b*, AP5-insensitive calcium accumulations previously observed at moderate frequency synaptic stimulation<sup>17</sup> are indicated by the patterned region. In most experiments the stimulating electrode was placed 300–500  $\mu\text{m}$  from the cell in distal stratum radiatum (position S1), activating fibres synapsing on the circled region (distal apical dendrites). This distal position facilitates measurements of calcium accumulations with minimal interference from AP5-insensitive accumulations. The cell diagram is a coarse sketch from a fluorescence image of the cell in Fig. 2.

**METHODS.** Slice preparation and maintenance followed standard procedures<sup>30</sup>. Electrophysiological and imaging techniques were similar to those previously described<sup>17</sup>. Individual pyramidal cells were iontophoretically filled with fura-2 (–1 nA, 5 min). The electrode was removed and 30–60 min allowed for the dye to diffuse to distal dendrites. From comparisons of cell soma fluorescence with that of calibration solutions, intracellular fura-2 concentrations were estimated to be 50–150  $\mu\text{M}$ . Cells with higher fura-2 levels showed diminished AP5-sensitive accumulations, and the time courses of all accumulations were slower. An extracellular electrode recorded the population spike evoked by 0.1 Hz test pulses. For all cells used in the imaging experiments reported here, nearby field potentials displayed LTP (at least a 50% increase in the amplitude of the population spike that reached a stable baseline 10 min after high frequency stimulation). Stimulus trains of 100 Hz for 0.8–1.0 s produced a persistent increase in amplitude of the population spike, from a prestimulation value of  $320 \pm 180 \mu\text{V}$  to  $810 \pm 370 \mu\text{V}$  ( $n=20$ ) for stratum radiatum stimulation and from an average of  $250 \mu\text{V}$  to  $710 \mu\text{V}$  ( $n=4$ ) for stratum oriens stimulation. Field-potential measurements of presynaptic volley amplitude made at 50  $\mu\text{m}$  intervals along the length of imaged cells showed that activated fibres were generally confined to dendritic regions (Fig. 1), with presynaptic volley amplitude evoked by stratum radiatum stimulation typically 20 times larger in distal stratum radiatum than in stratum oriens. Experiments conducted with AP5-containing saline used 100  $\mu\text{M}$  DL-AP5 (Sigma) or 50–100  $\mu\text{M}$  D-AP5 (Sigma) with 25–30 min for washing out.

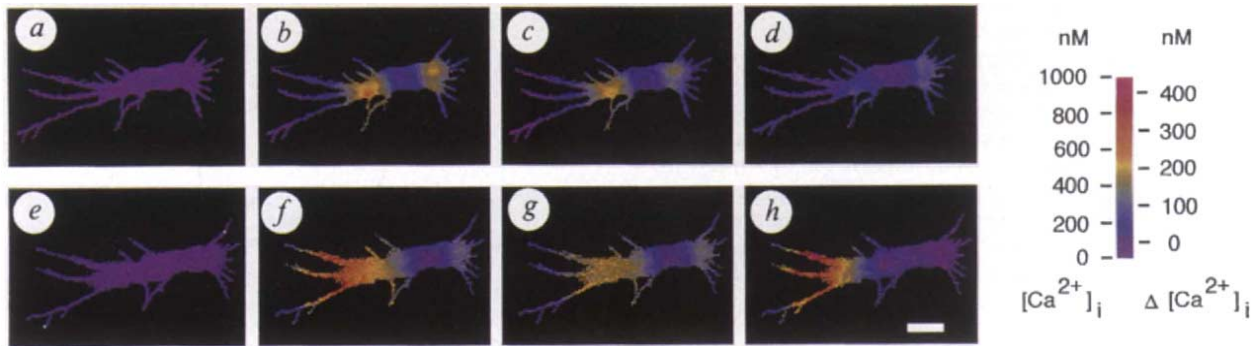


FIG. 2 High-frequency stimulations produced AP5-sensitive accumulation in dendritic regions postsynaptic to activated afferents. A stimulating electrode in position S1 (Fig. 1) delivered stimulus trains of 100 Hz (1 s) or 20 Hz (5 s) in control- and AP5-containing saline. Calcium levels were computed from ratios of 340 nm and 380 nm fluorescence images. The camera lucida-like masks that define pixels where the calcium concentration is displayed in pseudocolour were produced from 380 nm excited fluorescence intensity profiles. Slight differences in the masks result from slight differences in the focus position for the two experiments. *a, e*, Resting calcium distribution in the absence of stimulation. *b*, Calcium accumulation in the proximal apical and basal dendrites produced by 20 Hz stimulation of afferent fibres (map computed from images taken from  $t=4-5$  sec from the start of the stimulation) in control saline, and *c*, in the presence of AP5. *d*, Image produced by pixel-by-pixel subtraction of distribution in AP5-containing saline (*c*) from corresponding distribution in control saline (*b*) reveals no AP5-sensitive component for 20 Hz stimulation. (Calcium accumulations showed small trial-to-trial variation and the small AP5-sensitive component in the basal dendrites in (*d*) was not statistically reliable.) *f*, Distribution produced in control saline during 100-Hz, 1-s afferent stimulation (map computed from images taken from  $t=0-630$  ms from the

start of the stimulation). *g*, Distribution under identical conditions as *f*, but in the presence of AP5. *h*, Image produced by pixel-by-pixel subtraction of distribution in AP5-containing saline (*g*) from the corresponding distribution in control saline (*f*) shows a large AP5-sensitive accumulation during the tetanus in the area directly postsynaptic to the activated afferent fibres. The scale to the left of the colour bar refers to: *a-c, e-g*, and the scale to the right of the colour bar refers to *d* and *h*. Scale bars, 100  $\mu\text{m}$ .

**METHODS.** In experiments that compared accumulations in AP5-containing and control saline, protocols similar to those previously described<sup>31</sup> were used to eliminate the complication of changes in accumulation caused by the potentiation: (1) cells were stimulated and measured in AP5 followed by a second stimulation/measurement sequence in control saline; (2) the stimulated pathway was fully pre-potentiated by pre-imaging stimulus trains. In some experiments cells were tested in control saline followed by AP5-containing saline without explicit prepotentiation with no qualitative differences in results, suggesting that the potentiation of transmission only marginally affects the calcium accumulations under the stimulus conditions we used.

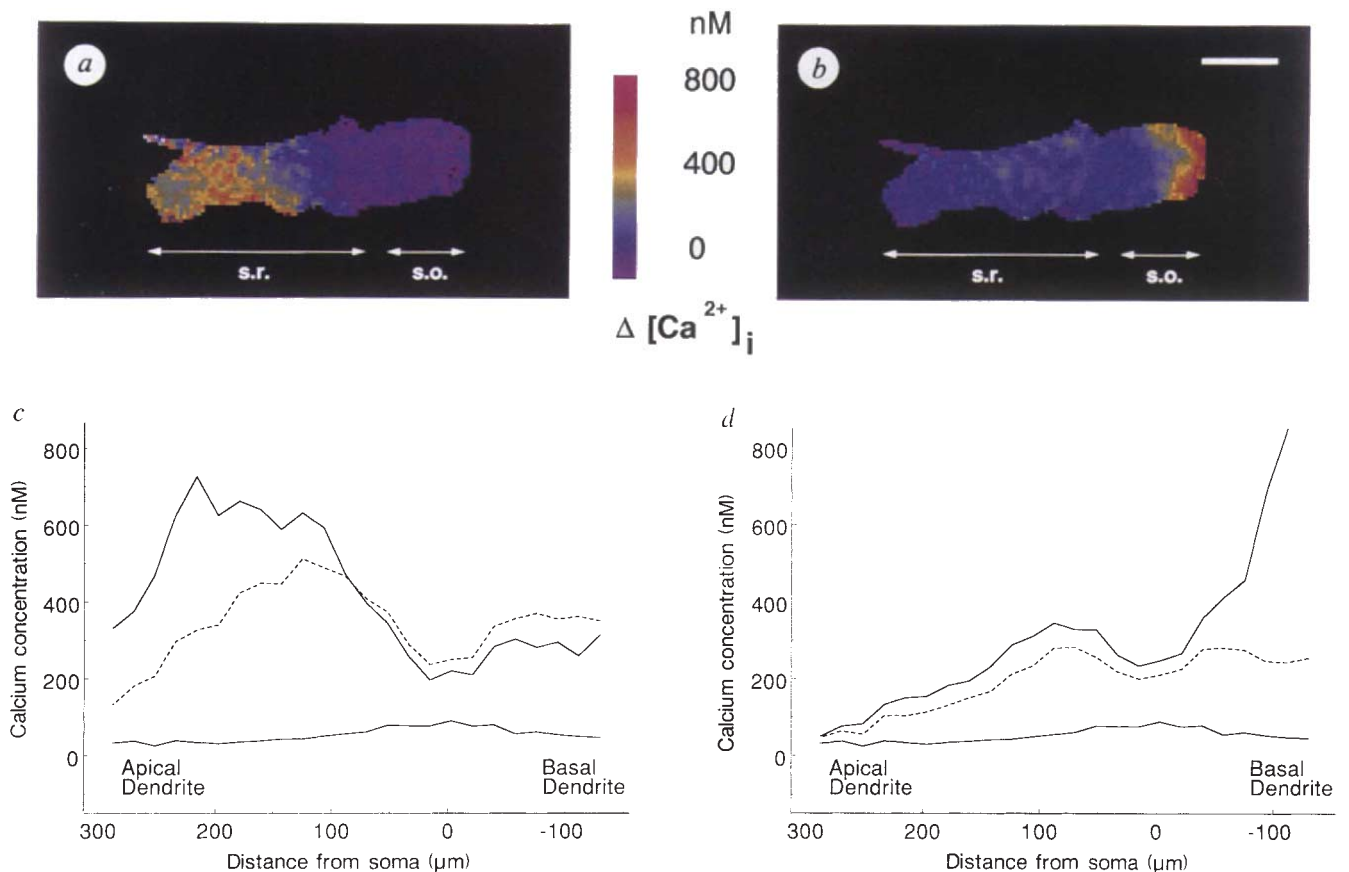


FIG. 3 AP5-sensitive accumulations correspond to terminal fields of stimulated afferent fibres. *a, b*, Difference maps (produced as in Figs 1*d* and *h*) representing the AP5-sensitive component of calcium accumulation produced by 100 Hz, 1 s stimulation of afferents in *a*, distal stratum radiatum and *b*, stratum oriens. *c, d*, Calcium accumulation in dendritic regions plotted against distance from the cell soma centre in the presence of AP5 (dashed

lines) and in control saline (solid line), with resting calcium levels also plotted (lowest solid line); *c*, stratum radiatum stimulation; *d*, stratum oriens stimulation. The difference between the line plot for control saline and the corresponding plot for AP5-containing saline represents the AP5-sensitive component shown for all cell locations in the two-dimensional maps in Fig. 3*a, b*. Scale bars, 100  $\mu\text{m}$ .

### AP5. The results directly confirm the calcium rise predicted by NMDA receptor models of LTP induction.

Optical measurements of intracellular free calcium were performed on pyramidal cells in region CA1 of guinea pig hippocampal slices microinjected with the fluorescent calcium indicator fura-2 (ref. 18). A small group of afferent fibres was activated by electrical stimulation with a small bipolar electrode positioned in distal regions of stratum radiatum, 200–350  $\mu\text{m}$  from the cell-body layer (S1; Fig. 1a). Because activated fibres run predominantly parallel to the cell-body layer (stratum pyramidale) and diverge only several hundred micrometres over the electrode–cell distances used in our experiments<sup>19</sup>, calcium accumulation produced by influx through postsynaptic calcium-permeable channels near the presynaptic terminals of the activated afferents should be observed in distal apical dendritic regions (circled in Fig. 1b). It has been demonstrated in recent experiments<sup>17</sup> that with moderate frequency (20-Hz) tetanic stimulation of afferent fibre tracts, the most prominent calcium accumulations observed with fura-2 charge-coupled device imaging (1–2 s exposure times) occur in the proximal apical and basal dendrites (Fig. 1b). These AP5-insensitive accumulations are not specific to the dendritic areas that intersect the activated afferents and are probably produced by non-NMDA voltage-dependent calcium channels on the proximal apical and basal dendrites activated by stimulus-induced postsynaptic depolarization. Small AP5-sensitive components of accumulation were observed in postsynaptic dendrites near activated afferent fibres in some experiments, but these accumulations were not statistically reliable for 20 Hz stimulation.

The amplitude and reliability of LTP induction increase with stimulus frequency in the range 0–100 Hz<sup>20</sup>. Computer simulations suggest superlinear increases of NMDA receptor-mediated postsynaptic calcium accumulations with increasing stimulus frequency<sup>21</sup>. By increasing the temporal resolution of our calcium measurements and increasing the stimulation frequency, we could perform microfluorimetric measurements under conditions more fully optimized for observing NMDA-mediated calcium accumulations. For moderate stimulation (20 Hz for 5 s), our measurement techniques could reliably resolve only an AP5-insensitive component of accumulation in the proximal apical and basal dendrites<sup>17</sup> (Fig. 2b–d). High-frequency stimulation (100 Hz, 1 s) however, resulted in a qualitatively different additional component of accumulation (Fig. 2f) which is greatly reduced in AP5-containing saline (Fig. 2g). The difference map (Fig. 2h) shows that there is a large, localized AP5-sensitive increase in intracellular free calcium in the dendritic zone that intersects the group of activated afferent fibres. This localized calcium accumulation was observed in 19 out of 20 cells with brief (100-Hz) stimulation. Although we could not determine whether each imaged cell experienced LTP, field potential recordings near the imaged cell demonstrated robust LTP of the population spike in all cases (Fig. 2, methods). The average calcium accumulation in distal apical dendrites near stimulated afferents increased from  $170 \pm 80$  nM in AP5-containing saline to  $510 \pm 230$  nM in control saline ( $n = 20$ ). By contrast, basal dendrites showed no AP5-sensitive component: the average accumulation was  $300 \pm 150$  nM in AP5-containing saline and  $320 \pm 130$  nM in control saline. These values are computed from the fluorescent light temporally averaged over the 185 ms required for each image exposure and spatially averaged over a scale of several micrometres: they must be interpreted as an estimated temporal average of the combined calcium changes in both smooth dendrite and dendritic spines.

We next examined whether spatial localization of AP5-sensitive accumulations was dependent on the proximity of activated afferents rather than simply reflecting non-synaptic calcium channels of distal apical dendrites activated by high frequency afferent input. Experiments were conducted with two stimulating electrodes, one activating fibres in stratum radiatum (S1 of Fig.

1a; stimulation of distal apical dendrites), the other activating fibres on the opposite side of the cell body in stratum oriens (S2 of Fig. 1a; stimulation of basal dendrites). Calcium distributions were determined as the cell was synaptically activated with 100 Hz, 0.8 s stimulus trains in either stratum oriens or stratum radiatum, measured in both control saline and AP5-containing saline. For stratum radiatum stimulation (as in Fig. 2h), there was a large AP5-sensitive component of calcium accumulation localized to distal apical dendrites (Fig. 3a, c) However, for stratum oriens stimulation in the same cell there was a large AP5-sensitive accumulation localized to the basal dendrites (Fig. 3b, d). The localization of AP5-sensitive accumulations to the region receiving the activated afferents with smaller AP5-insensitive accumulations located in the proximal apical and basal dendrites was observed in all experiments ( $n = 4$ ) comparing stratum radiatum versus stratum oriens stimulation.

To complement the high spatial resolution CCD images, a low spatial resolution photodiode array and single wavelength fluorescence methods (Fig. 4, methods) were used to provide higher temporal resolution measurements of calcium accumulation. Four photodiodes measured fluorescence from  $45 \mu\text{m} \times 45 \mu\text{m}$  areas on basal dendrites, soma, proximal apical dendrites and distal apical dendrites (Fig. 4A). Figure 4B(a–d), shows the time course and AP5-dependence of calcium accumulations at these locations produced by 100 Hz, 1 s activation of an afferent fibre tract that intersected distal apical dendrites. At all dendritic locations a rapid rise in calcium was observed that

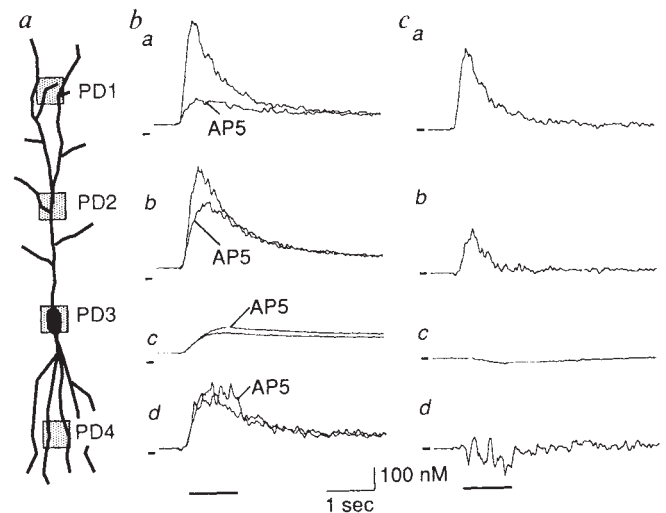


FIG. 4 A, Higher time-resolution measurements of calcium accumulations in four cell areas (PD1–PD4). Individual photodiodes collected fluorescence from a region corresponding to  $45 \mu\text{m} \times 45 \mu\text{m}$  areas on the cell image and were separated by  $170 \mu\text{m}$ . B, The time course of calcium concentration changes produced by 100 Hz, 1 s stimulation of afferent tracts intersecting the distal apical dendrite in control saline and AP5-containing saline in a, distal apical dendrite (PD1); b, proximal apical dendrite (PD2); c, soma (PD3); and d, basal dendrite (PD4). C, AP5-sensitive components of accumulation produced by subtracting the time course of calcium concentration changes in AP5-containing saline from the corresponding time course in control saline for each of the photodiode locations.

**METHODS.** Photodiode measurements of calcium concentration were made with an array consisting of four photodiodes (Hamamatsu S1087-01) operating in photoconduction mode. Photocurrents were individually amplified (response time: 25 ms) and simultaneously sampled by a microcomputer. Shortly before stimulation, resting calcium concentrations were determined from standard 340 nm, 380 nm ratio measurements of fluorescence at each photodiode. Continuous measurement of fluorescence intensity from constant 380 nm illumination commenced shortly before tetanic stimulation of the Schaffer collateral pathway. Calcium concentrations were computed from the ratio-determined pre-stimulus calcium concentration and the changes in 380 nm fluorescence during the stimulus train by the single wavelength method (see ref. 18; equation 6).

peaked within 200 ms of the onset of the stimulus train, decreasing substantially during the remaining stimulus period. (A commensurate decrease in the population spike amplitude measured during 100-Hz stimulation occurs during this decreasing calcium phase, suggesting reduced postsynaptic cell spiking and depolarization). Accumulations in the soma were somewhat slower and smaller. In AP5 there is a dramatic decrease in the amplitude of the accumulation in distal apical dendrites, the location of afferent stimulation, with little change observed in the accumulation in the basal dendrites. Subtraction of the accumulation measured in AP5 from that in control saline for each photodiode (Fig. 4C a-d) reveals the time course of the AP5-sensitive component of accumulation. All cells tested ( $n = 5$ ) showed large AP5-sensitive calcium accumulations in dendritic regions receiving afferents activated at high frequency. The average peak calcium accumulation (spatially averaged over the  $45 \mu\text{m} \times 45 \mu\text{m}$  photodiode collection area) in distal apical dendrites near the stimulated afferent fibres increased from 160 nM in AP5-containing saline to 860 nM in control saline, and in several cases reached levels that saturated the fura-2 signal. By contrast, basal dendrites showed only a small AP5-sensitive component (possibly because of enhanced depolarization of voltage-dependent calcium channels): the spatially averaged peak accumulation was 360 nM in AP5-containing saline and 450 nM in control saline.

On the basis of AP5-sensitivity, calcium accumulations observed during synaptic activation can be divided into two components. AP5-insensitive accumulations widely distributed over the apical and basal dendritic trees are produced in response to moderate and high-frequency stimulus trains. Such accumulations could, in principle, play the part of a second messenger in postsynaptic modifications such as heterosynaptic long-term depression<sup>22</sup> or in anti-hebbian reductions in synaptic strength<sup>23-25</sup>. These occur in proximal dendrites regardless of stimulus electrode position, but it is not known if any component of this accumulation is enhanced or localized to dendritic regions near activated afferents. The AP5-sensitive calcium accumulations are strikingly different. They are localized to synaptically activated dendritic regions, verifying a central prediction of the NMDA receptor-mediated induction theory that a pool of calcium is selectively produced that could act locally, either via enzyme activation<sup>26,27</sup> or some other mechanism<sup>28,29</sup>, to potentiate only those synapses activated during a high-frequency tetanus. These accumulations are much larger and more reliably observed as the stimulus frequency increases from 20–100 Hz, in parallel with the frequency-dependent efficacy of LTP induction and consistent with computer simulations of NMDA receptor-mediated calcium accumulations<sup>21</sup>. AP5-sensitive accumulations reach their peak at about 200 ms (20 stimulus pulses) after the beginning of high-frequency activation, consistent with the observation that repeated brief trains of high-frequency stimuli are very effective at LTP induction. □

Received 5 February; accepted 6 April 1990.

- Lynch, G., Larson, J., Kelso, S., Barrionuevo, G. & Schottler, F. *Nature* **305**, 719–721 (1983).
- Malenka, R. C., Kauer, J. A., Zucker, R. S. & Nicoll, R. A. *Science* **242**, 81–84 (1988).
- Bliss, T. V. P. & Lomo, T. *J. Physiol., Lond.* **232**, 331–356 (1973).
- Collingridge, G. L., Kehl, S. J. & McLennan, H. *J. Physiol., Lond.* **334**, 19–31 (1983).
- Nowak, L., Bregestovski, P., Ascher, P., Herbert, A. & Prochiantz, A. *Nature* **307**, 462–465 (1984).
- Mayer, M. L., Westbrook, G. L. & Guthrie, P. B. *Nature* **309**, 261–263 (1984).
- MacDermott, A. B., Mayer, M. L., Westbrook, G. L., Smith, S. J. & Barker, J. L. *Nature* **321**, 519–522 (1986).
- Jahr, C. E. & Stevens, C. F. *Nature* **325**, 522–525 (1987).
- Mayer, M. L. & Westbrook, G. L. *J. Physiol., Lond.* **394**, 501–527 (1987).
- Nowak, L. & Nowak, L. *J. Physiol., Lond.* **399**, 247–266 (1988).
- Bliss, T. V. P. & Lynch, M. A. in *Long-Term Potentiation: From Biophysics to Behavior* (eds Landfield, P. W. & Deadwyler, S. A.) 3–72 (Liss, New York, 1988).
- Wigstrom, H. & Gustafsson, B. in *Long-term Potentiation: From Biophysics to Behavior* (eds Landfield, P. W. & Deadwyler, S. A.) 73–107 (Liss, New York, 1988).
- Nicoll, R. A., Kauer, J. A. & Malenka, R. C. *Neuron* **1**, 97–103 (1988).
- Brown, T. H., Chapman, P. F., Kairiss, E. W. & Keenan, C. L. *Science* **242**, 724–728 (1988).
- Collingridge, G. L. & Davies, S. N. in *The NMDA Receptor* (eds Watkins, J. C. & Collingridge, G. L.) 123–135 (Oxford University Press, 1989).
- Tank, D. W., Sugimori, M., Connor, J. A. & Llinás, R. *Science* **242**, 773–777 (1988).
- Regehr, W. G., Connor, J. A. & Tank, D. W. *Nature* **341**, 533–536 (1989).

- Grynkiewicz, G., Poenie, M. & Tsien, R. Y. *J. Biol. Chem.* **260**, 3440–3450 (1985).
- Andersen, P., Silfvenius, H., Sundberg, S. H. & Sveen, O. *J. Physiol., Lond.* **307**, 273–299 (1980).
- Dunwiddie, T. & Lynch, G. *J. Physiol., Lond.* **276**, 353–367 (1978).
- Holmes, W. R. & Levy, W. B. *J. Neurophysiol.* (in the press).
- Lynch, G. S., Dunwiddie, T. & Gribkoff, V. *Nature* **266**, 737–739 (1977).
- Levy, W. B. & Steward, O. *Neuroscience* **8**, 791–797 (1983).
- Stanton, P. K. & Sejnowski, T. *J. Nature* **339**, 215–218 (1989).
- Lisman, J. *Proc. natn. Acad. Sci. U.S.A.* **86**, 9574–9578 (1989).
- Malinow, R., Schulman, H. & Tsien, R. W. *Science* **245**, 862–866 (1989).
- Malenka, R. C. *et al. Nature* **340**, 554–557 (1989).
- Rall, W. & Rinzel, J. *Biophys. J.* **13**, 648–688 (1973).
- Rall, W. & Segev, I. in *Computer Simulation in Brain Science* (eds Cotterill, R. M. J.) 26–43 (Cambridge University Press, 1988).
- Schwartzkroin, P. A. *Brain Res.* **85**, 423–436 (1975).
- Collingridge, G. L., Herron, C. E. & Lester, R. A. J. *J. Physiol., Lond.* **399**, 301–312 (1988).

## Stimulation of protein tyrosine phosphorylation by the B-lymphocyte antigen receptor

Michael R. Gold, Debbie A. Law  
& Anthony L. DeFranco\*

The George Williams Hooper Foundation and the Department of Microbiology and Immunology, The University of California, San Francisco, San Francisco, California 94143-0552, USA

**SIGNALLING by membrane immunoglobulin, the B-lymphocyte antigen receptor, regulates B-cell maturation and activation. Crosslinking of membrane immunoglobulin by antigen or by anti-immunoglobulin antibodies inactivates immature B cells, eliminating many of the B cells capable of producing auto-antibodies<sup>1</sup>. By contrast, crosslinking of membrane immunoglobulin promotes activation of mature B cells for clonal expansion and antibody production against foreign antigens<sup>2</sup>. Crosslinking membrane IgM on the immature B-cell line WEHI-231 induces growth arrest<sup>3</sup>. This response may be analogous to the deletion or inactivation of immature B cells that is induced by antigen or anti-IgM antibodies. Membrane immunoglobulin crosslinking stimulates phosphoinositide hydrolysis, which leads to increases in intracellular calcium and activation of protein kinase C<sup>4-6</sup>. The induced phosphoinositide breakdown is important for inhibiting WEHI-231 growth (ref. 7 and D. Page, M.R.G., K. Fahey, L. Matsuuchi and A.L.D., manuscript submitted for publication), but may not be sufficient, as agents that elevate calcium and activate protein kinase C cause only partial growth arrest<sup>7</sup>. We now show that in both mature splenic B cells and the immature B-cell line WEHI-231 crosslinking membrane immunoglobulin also stimulates phosphorylation of protein tyrosine, a reaction that has been implicated as a key regulator of cell growth. Most of these phosphorylations were not a consequence of the phosphoinositide pathway. Thus, tyrosine phosphorylation is a second mode of transmembrane signalling by membrane immunoglobulin.**

Immunoblot analysis using a monoclonal anti-phosphotyrosine antibody showed that membrane immunoglobulin (mIg) crosslinking induced a rapid increase in protein tyrosine phosphorylation in WEHI-231 cells (Fig. 1a). Within 1–2 min, increased tyrosine phosphorylation of Triton X-100-soluble polypeptides with relative molecular mass of 150,000–200,000 ( $M_r$  150–200K) (four or five bands), 123–129K (a doublet), 101K, 85–90K (two minor bands), 81K, 69–73K, (four bands), and 42K was observed. Maximal phosphorylation occurred within 5–10 min of adding anti-IgM antibodies. Several other polypeptides (two of  $M_r$  59–61K and a minor band at 51K) were tyrosine phosphorylated with slower kinetics. Increased tyrosine phosphorylation was still evident after 1 h of stimulation with anti-IgM antibodies, although for several polypeptides it had declined. Anti-IgM treatment also increased tyrosine phosphorylation of several polypeptides in the Triton X-100-

\* To whom correspondence should be addressed.